New Miniaturized Dual-Mode Dual-Band Ring Resonator Bandpass Filter With Microwave *C*-Sections

***Abstract*—A new miniaturized dual-mode dual-band ring resonator bandpass filter is implemented by a cascade of several microwave *C*-sections. Each *C*-section is used to substitute a transmission line section of designated electrical length. Through proper design of input/output coupling configuration, two transmission zeros can be created on both sides of each passband. Two circuits with four and six microwave *C*-sections are fabricated for confirmation. They occupy less than 30% of the area of a traditional ring resonator filter. Measured responses agree very well with the simulation.**

***Index Terms*—Bandpass filter, dual-band, dual-mode, microwave *C*-section, miniaturized.**

I. Introduction

RING RESONATOR filters have been widely used in front-ends of microwave systems due to their compact size and easy design [1-3]. The circuit in [1] could be the first ring resonator bandpass filter with two degenerate modes that are of essential importance for constituting the passband. The quasi-elliptic bandpass filter in [2] is designed to have tunable transmission zeros with a constant bandwidth. In [3], a periodic stepped-impedance ring resonator is devised to develop a miniaturized dual-mode filter with a wide upper stopband. Notice that all these circuits involve bandpass filters with a single passband.

Recently, rapid development of modern wireless systems, such as GSM and WLAN, has created a need for dual-band RF devices. Several dual-mode dual-band bandpass filters have been published [4-8]. In [4], the stacked-loop structure consists of two dual-mode rings on different layers and each ring resonator controls one passband. Based on a similar idea, an alternative dual-band filter with a coplanar waveguide (CPW) feed line is carried out in [5]. In [6], a loop resonator is proposed for a planar dual-band filter. The feed lines are placed between two resonators to offer sufficient coupling for both passbands. The dual-band filter in [7] is designed in a multilayer structure consisting of dual-mode resonators in a reflector cavity. It is noted that each selected passband in [4]-[7] is mainly controlled by a resonator. The dual-mode dual-band filter in [8] is contrived with a single stepped-impedance ring resonator.

In this paper, a dual-mode dual-band bandpass filter is implemented with microwave-*C* sections, which have nonlinear phase shift property in frequency [9] and are suitable for development of dual-band devices [10]. Here, each microwave *C*-section is used to substitute a λ/4- or λ/6-section of a traditional ring. Analysis will be conducted and design curves plotted for facilitating the circuit realization. Emphasis is also put on the input/output configuration for creating transmission zeros on both sides of each passband. Two circuits are simulated, fabricated and measured for confirmation.

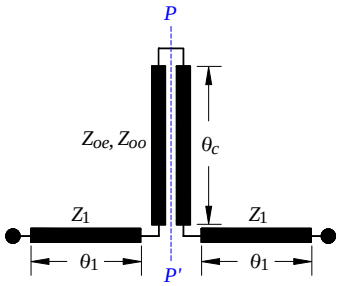

Fig. 1. The microwave-*C* section for substituting a transmission line section.

II. Formulation

Fig. 1 shows the elementary two-port for constructing the dual-mode dual-band filter. It consists of two transmission line sections of length θ_1 and characteristic impedances Z_1 with a microwave *C*-section of electric length θ_c in between. In our approach, a uniform ring is treated as a cascade of N identical sections and each of them will be implemented by the network in Fig. 1. Then, let the two designated frequencies be f_1 and $f_2 = nf_1$, and the characteristic impedance of the ring peripheral be Z_u. For simplicity, $Z_1 = Z_u = \sqrt{Z_{oe}Z_{oo}}$ is chosen, where Z_{oe} and Z_{oo} are the even- and odd-mode characteristic impedances of the coupled-line. By enforcing the *ABCD* matrix of the two-port to be equal to those of a uniform section of $\theta_u = 2\pi/N$ and $2\theta_u$ at f_1 and f_2, respectively, the following four equations can be readily obtained:

$$F(\theta_c)\cos 2\theta_1 + 2Z_1 \sin 2\theta_1 = E(\theta_c)\cos\theta_u \quad (1a)$$

$$F(\theta_c)\sin 2\theta_1 - 2Z_1 \cos 2\theta_1 = E(\theta_c)\sin\theta_u \quad (1b)$$

$$F(n\theta_c)\cos 2n\theta_1 + 2Z_1 \sin 2n\theta_1 = E(n\theta_c)\cos 2\theta_u \quad (1c)$$

$$F(n\theta_c)\sin 2n\theta_1 - 2Z_1\cos 2n\theta_1 = E(n\theta_c)\sin 2\theta_u \quad (1d)$$

where

$$E(\varphi) = -Z_{oe}\cot\varphi - Z_{oo}\tan\varphi \quad (2a)$$

$$F(\varphi) = -Z_{oe}\cot\varphi + Z_{oo}\tan\varphi \quad (2b)$$

Based on (1) and (2), Fig. 2 plots z_{oe}, z_{oo} and θ_c as functions of n for $\theta_u = 60^o$ with $\theta_1 = 14^o$ and $\theta_u = 90^o$ with $\theta_1 = 24^o$. Here, $Z_1 = 85\ \Omega$ is chosen and z_{oe} and z_{oo} are respectively Z_{oe} and Z_{oo} normalized with respect to $Z_o = 50\ \Omega$, the reference port impedance. Such a high Z_1 is chosen since narrow lines are capable of providing sufficient coupling to our dual-band design. In Fig. 2, z_{oe} and z_{oo} gradually decrease and increase, respectively, when n is increased from 1.5 to 2. It is noted that when $n = 2$, the C-section has $z_{oe} = z_{oo}$. This means that the two-port becomes a folded uncoupled section at $f_2 = 2f_1$, which in turns implies that our structure is limited to $n \le 2$.

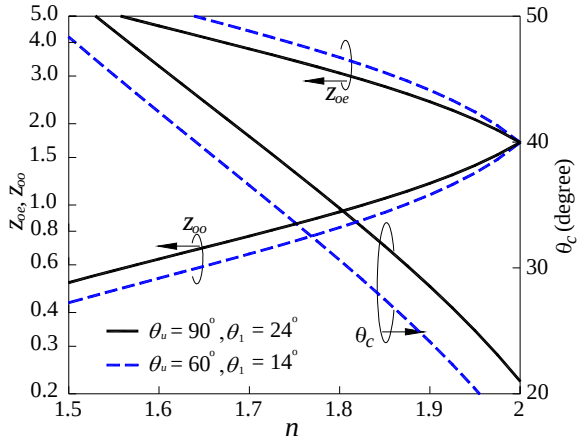

Fig. 2. z_{oe}, z_{oo} and θ_c as functions of n.

TABLE I CONTROL OF TWO BANDWIDTHS WITH A_{P1} AND A_{P2}

A_{p1} (mm^2)	A_{p2} (mm^2)	f_1 (GHz)		f_2 (GHz)	
		even	*odd*	*even*	*odd*
1.2×0.418	0.715×0.4	2.53	2.56	4.53	4.68
1.7×0.418	0.715×0.4	2.50	2.56	4.40	4.68
2.3×0.418	0.715×0.4	2.45	2.56	4.25	4.68
1.7×0.418	0.6×0.4	2.50	2.57	4.44	4.68
1.7×0.418	0.8×0.4	2.50	2.54	4.35	4.68
1.7×0.418	1.0×0.4	2.50	2.5	4.23	4.68

III. IMPLEMENTATION, SIMULATION AND MEASUREMENT

Fig. 3(a) depicts the layout of the filter with four C-sections on a substrate with $\varepsilon_r = 10.2$ and thickness = 1.27 mm. The perturbation patches A_{p1} and A_{p2} are used to split off the degenerate modes at the two designated frequencies ($f_1 = 2.44$ GHz and $f_2 = 4.49$ GHz). Fig. 3(b) plots the simulated results [12] with $\ell_{c1} = \ell_{c2} = 0$ for testing the electrical length θ_S (evaluated at f_1), where the circuit is weakly coupled by the feed lines. One can see that all $|S_{21}|$ curves possess a dual-resonance response at f_1 and f_2 with two transmission zeros on both the upper and lower sides. Note that only one resonant peak exists and no zero around f_2 when $\theta_S = 90^o$, since one of the two degenerate modes has null voltage at the excitation position and it is not activated. Herein, $\theta_S = 60^o$ rather than 45^o is used since enough space should be saved for ℓ_{c1}.

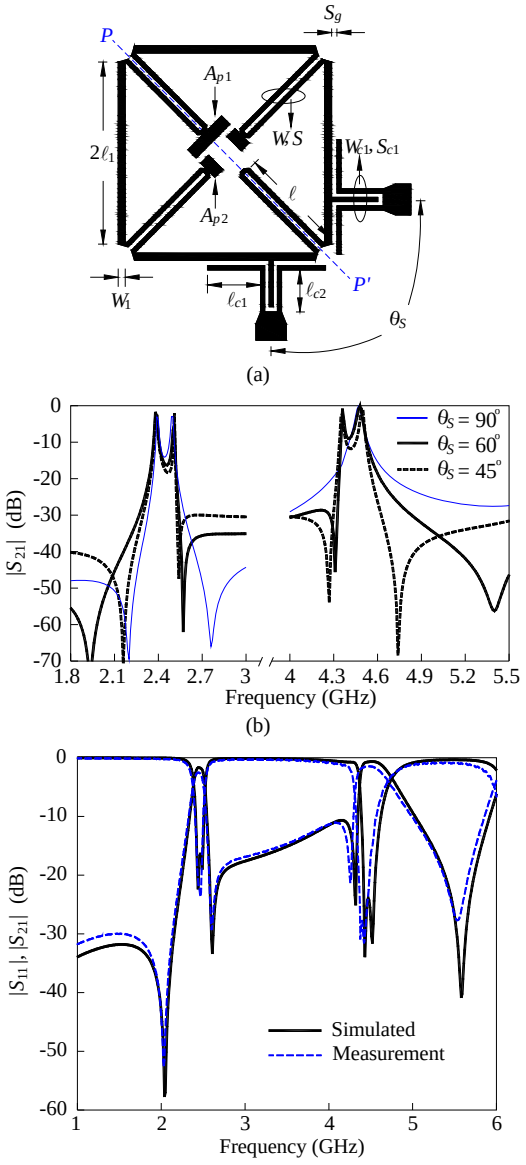

Fig. 3. Filter with four C-sections. (a) Circuit layout. (b) $|S_{21}|$ response with $\ell_{c1} = \ell_{c2} = 0$. (c) Simulated and measured results. Circuit dimensions in mm: $S = 0.164$, $W_1 = 0.25$, $W = W_{c1} = S_{c1} = 0.15$, $S_g = 0.188$, $\ell = 3.81$, $\ell_1 = 3.23$, $\ell_{c1} = 1.57$, $\ell_{c2} = 1.5$. $A_{p1} = 1.7 \times 0.418$ mm^2, $A_{p2} = 0.715 \times 0.4$ mm^2.

Table I lists the resonant frequencies when the patches are changed, showing the control of the two bandwidths. The patches are placed at the two symmetric planes of the resonant modes. At f_1, A_{p1} can change the even mode frequency but has no influence on the odd mode, where the voltage is zero. This is exactly the same as the function of the perturbation patch in design of the traditional ring resonator filter [2]. The impact of the changes of A_{p2} on the resonance modes at f_1 and f_2 can be explained in a similar way.

The interdigital structure ($\ell_{c1} = 0$) is used to provide coupling from the feed line to the circuit. It is found that the first band needs more coupling to establish the passband. Increasing ℓ_{c1}, however, will decrease the bandwidth at f_2. We had such experience in developing the multi-mode filter in [11]. Then, A_{p2} are increased to compensate this effect. This will decrease the bandwidth at f_1; this in turns contributes a positive factor for establishing a passband with satisfactory return loss. Fig. 3(c) plots the simulated and measured results of the experimental circuit. The fractional bandwidths Δ_1 and Δ_2 at f_1 and f_2 are 3.03% and 6.97%. The measurement shows that the insertion losses are 2.56 dB and 1.45 dB, and return losses 23.5 dB and 26.4 dB in the first and the second passbands, respectively. The circuit occupies only 27.3% of the area of a traditional ring resonator filter designed at f_1.

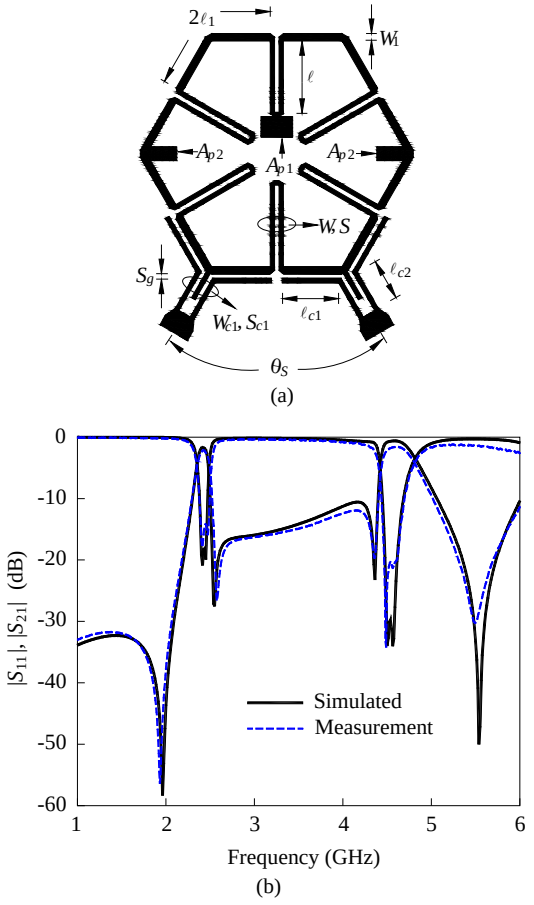

Fig. 4. Dual-mode dual-band bandpass filter with six microwave *C*-sections. (a) Circuit layout. (b) Simulated and measurement results. Circuit dimensions in mm: $W = 0.148$, $S = 0.157$, $W_1 = 0.25$, $W_{c1} = S_{c1} = S_g = 0.15$, $\ell = 2.51$, $\ell_1 = 2.01$, $\ell_{c1} = 1.94$, $\ell_{c2} = 1.44$. $A_{p1} = 1.1 \times 0.7$ mm^2, $A_{p2} = 0.9 \times 0.47$ mm^2. $\theta_S = 60^o$.

Fig. 4(a) plots the layout of the second dual-mode dual-band bandpass filter with six microwave sections, and Fig. 4(b) shows the simulated and measured results. The circuit is designed to have $f_1 = 2.42$ GHz and $f_2 = 4.61$ GHz with $\Delta_1 = 3.5\%$ and $\Delta_2 = 6.24\%$, respectively. At f_1 and f_2, the measured $|S_{21}|$ are 2.39 dB and 1.56 dB, respectively, and the in-band return losses are better than 15 dB. The transmission zeros are at 1.93 GHz, 2.57 GHz, 4.35 GHz and 5.49 GHz. The circuit has 29.1% of the area of a traditional ring filter. Good agreement between simulated and measured results can be observed.

IV. Conclusion

New miniaturized dual-mode dual-band ring resonator bandpass filters are developed by cascading the microwave *C*-sections. The circuits use less than one-third of the area of a conventional ring resonator bandpass filter designed at the first frequency. The two experimental circuits demonstrate good inband insertion losses and return losses. In addition, two transmission zeros are created on both sides of each passband. The shortcoming of this circuit structure is the limited tuning range of the second frequency.

References

[1] I. Wolff, "Microstrip bandpass filters using degenerate modes of a microstrip ring resonators," *Electron. Lett.*, vol. 8, no. 12, pp. 163-164, Jun. 1972.

[2] A. C. Kundu and I. Awai, "Control of attenuation pole frequency of a dual-mode microstrip ring resonator bandpass filter," *IEEE Trans. Microw. Theory Tech.*, vol. 49, no. 6, pp. 1113-1117, Jun. 2001.

[3] J.-T. Kuo and C.-Y. Tsai, "Periodic stepped-impedance ring resonator (PSIRR) bandpass filter with a miniaturized area and desirable upper stopband characteristics," *IEEE Trans. Microw. Theory Tech.*, vol. 54, no. 3, pp. 1107-1112, Mar. 2006.

[4] J.-X. Chen, T.-Y. Yum J.-L. Li and Q. Xue, "Dual-mode dual-band bandpass filter using stacked-loop structure," *IEEE Microw. Wireless Compon. Lett.*, vol. 16, no. 9, pp. 502-504, Sep. 2006.

[5] X. Y. Zhang and Q. Xue, "Novel dual-mode dual-band filters using coplanar-waveguide-fed ring resonators," *IEEE Trans. Microw. Theory Tech.*, vol. 55, no. 10, pp. 2183-2190, Oct. 2007.

[6] A. Görür and C. Karpuz, "Compact dual-band bandpass filters using dual-mode resonators," in *IEEE MTT-S Int. Micro. Sym. Dig*., Jun. 2007, pp. 905-908.

[7] C. Lugo and J. Papapolymerou, "Multilayer dual-band filter using a reflector cavity and dual-mode resonators," *IEEE Microw. Wireless Compon. Lett.*, vol. 17, no. 9, pp. 637-639, Sep. 2007.

[8] T.-H. Huang, H.-J. Chen, C.-S. Chang, L.-S. Chen, Y.-H. Wang and M.-P. Houng, "A novel compact ring dual-mode filter with adjustable second-passband for dual-band applications," *IEEE Microw. Wireless Compon. Lett.*, vol. 16, no. 6, pp. 360-362, Jun. 2006.

[9] B. M. Schiffman, "A new class of broad-band microwave 90-degree phase shifter," *IRE Trans. Microw. Theory Tech.*, vol. 6, no. 6, pp. 232-237, Apr. 1958.

[10] Y.-C. Chiou, J.-T. Kuo, and C.-H. Chan, "New miniaturized dual-band rat-race coupler with microwave *C*-sections," in *IEEE MTT-S Int. Micro. Sym. Dig*., Jun. 2009, pp. 701-704.

[11] Y.-C. Chiou, J.-T. Kuo, and E. Cheng, "Broadband quasi-Chebyshev bandpass filters with multimode stepped-impedance resonators (SIRs)," *IEEE Trans. Microw. Theory Tech*., vol. 54, no. 8, pp. 3352-3358, Aug. 2006.

[12] *IE3D Simulator*, Zeland Software Inc., Jan. 1997.

New Miniaturized Dual-Band Rat-Race Coupler With Microwave *C*-Sections

***Abstract*—Based on microwave *C*-sections, rat-race coupler is designed to have a dual-band characteristic and a miniaturized area. The *C*-section together with two transmission line sections attached to both of its ends is synthesized to realize a phase change of 90° at the first frequency, and 270° at the second passband. The equivalence is established by the transmission line theory, and transcendental equations are derived to determine its structure parameters. Two circuits are realized in this presentation; one is designed at 2.45/5.2 GHz and the other at 2.45/5.8 GHz. The latter circuit occupies only 31% of the area of a conventional hybrid ring at the first band. It is believed that this circuit has the best size reduction for microstrip dual-band rat-race couplers in open literature. The measured results show good agreement with simulation responses.**

***Index Terms*—Microwave *C*-section, dual-band, microstrip line, miniaturization, rat-race coupler.**

I. Introduction

In the RF frond-end of a modern communication system, hybrid couplers are one of the most important devices [1]. They are widely used in several microwave and millimeter wave sub-systems such as balanced amplifiers and mixers. In the past few decades, a series of innovative synthesis and design have been proposed for these couplers [2]-[5]. In [2], simple formulation is devised to design the ring coupler. In [3], a rigorous synthesis procedure is demonstrated for branch-line couplers with equal power division. In [4], a rat-race coupler consisting of cascade structure of alternative high- and low-impedance transmission lines is presented to achieve a large power split ratio over a wide bandwidth. On the basis of design equations in [4], a miniaturized periodic stepped-impedance rat-race coupler with arbitrary power division ratio can be realized [5]. Note that all couplers in [2]-[5] are designed for operation at a single band.

Recent rapid progress in wireless communications has created a need of dual-band operation for RF devices, such as the global systems for mobile communication systems (GSM) at 0.9/1.8 GHz and wireless local area network (WLAN) at 2.4/5.2 GHz. Recently, numerous research topics on dual-band hybrid couplers have been published [6]-[13]. In [6], a planar dual-band branch-line coupler with a compact circuit area is proposed. Each quarter wavelength (λ/4) section is replaced by a short transmission line section with a pair of shunt short-circuited or open stubs attached to its ends. Based on a similar circuit structure, a rat-race coupler with two arbitrary operation frequencies is presented in [7]. An alternative branch-line coupler for dual-band operation is introduced in [8]. The circuit consists of cross branches that offer extra degrees of freedom to achieve the design. In [9], a tapped open stub is used to contrive a dual-band branch-line coupler. The two bands can be arbitrarily designated by adequately tuning the length and characteristic impedance of the stub. In [10], a stepped-impedance line section with two open stubs is proposed to establish a dual-band rat-race coupler. In [11], four identical open stubs are devised for design of a novel dual-band rectangular patch hybrid coupler.

The metamaterial approach [12]-[13] can also be used to implement couplers with the dual-band operation. In [12], arbitrary dual-band components such as branch-line and rat-race couplers are realized by composite right- and left-handed transmission line (CRLH TL) sections. Dual-band devices are also carried out on the basis of the simplified CRLH TL [13]. So far, however, it is still a challenge to design a miniaturized dual-band rat-race coupler. In [14], a novel circuit unit is utilized to design a dual-band branch line and rat-race coupler with arbitrary power division ratios. Each unit consists of a stepped-impedance line section with an open stubs tapped with its both ends. Rigorous design procedure is described and several circuits operating at 2.45/5.2 GHz are realized. To the best of our knowledge, it is the first miniaturized dual-band coupler with arbitrary power divisions at two designated bands in open literature.

In this paper, a miniaturized dual-band rat-race coupler is implemented with the microwave *C*-sections. Each λ/4 section of a conventional rat-race coupler is replaced by the proposed elementary two-port which consists of two line sections with a *C*-section in between. Design equations are formulated by establishing the equivalence between the two-port and the λ/4 section at two frequencies. To facilitate the circuit design, some design graphs are provided.

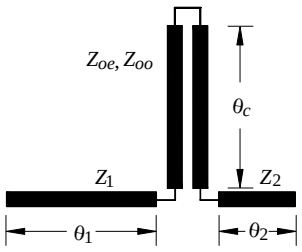

Fig. 1. The proposed elementary two-port with a *C*-section.

The presentation is organized as follows. In Sec. II, the dual-band characteristic of the proposed *C*-section is investigated and some design equations are formulated. Two circuits operating at 2.45/5.2 GHz and 2.45/5.8 GHz are fabricated and measured to validate the analysis. Sec. III demonstrates the simulation and measured results of these two experimental circuits, and Sec. IV draws the conclusion.

II. Elementary Two-Port for Dual-Band Operation

Figure 1 shows the proposed elementary two-port network for the dual-band operation. The two-port is built with two transmission line segments of lengths θ_1 and θ_2 and characteristic impedances Z_1 and Z_2 with a microwave *C*-section of length θ_c in between. Since the phase-shift of the *C*-section is nonlinear with respect to frequency [15], it is suitable for realizing the dual-band function.

Let the two designated operation frequencies be f_1 and $f_2 = nf_1$. In our approach, the six λ/4 sections of the traditional coupler are replaced by the proposed two-port. For simplicity, let $Z_1 = Z_2 = \sqrt{Z_{oe}Z_{oo}}$, where Z_{oe} and Z_{oo} are the even and odd mode characteristic impedances of the coupled-line. By enforcing the *ABCD* matrix of the two-port to be equal to those of a uniform transmission line section of 90° and 270° at f_1 and f_2, respectively, the following four equations can be readily obtained:

$$P(\theta_c)\cos\theta + 2Z_1\sin\theta = 0 \tag{1a}$$

$$P(\theta_c)\sin\theta - 2Z_1\cos\theta = Q(\theta_c)\times Z_T/Z_1 \tag{1b}$$

$$P(n\theta_c)\cos n\theta + 2Z_1\sin n\theta = 0 \tag{1c}$$

$$P(n\theta_c)\sin n\theta - 2Z_1\cos n\theta = -Q(n\theta_c)\times Z_T/Z_1 \tag{1d}$$

where

$$P(\theta_c) = Z_{oo}\tan\theta_c - Z_{oe}\cot\theta_c \tag{2a}$$

$$Q(\theta_c) = -(Z_{oo}\tan\theta_c + Z_{oe}\cot\theta_c) \tag{2b}$$

In (1) and (2), $\theta = \theta_1 + \theta_2$, Z_o is the reference impedance, and $Z_T = \sqrt{2}Z_o$ is the characteristic impedance of the six λ/4 sections of a conventional hybrid ring. After some algebraic manipulations, the following equations can be obtained for determination of Z_{oe} and Z_{oo}:

$$Z_T \times Z_{oe}(f_1) = Z_1^2\sec\theta\tan\theta_c + Z_1\tan\theta\tan\theta_c \tag{3a}$$

$$Z_T \times Z_{oo}(f_1) = Z_1^2\sec\theta\cot\theta_c - Z_1\tan\theta\cot\theta_c \tag{3b}$$

$$Z_T \times Z_{oe}(f_2) = Z_T Z_1\tan n\theta\tan n\theta_c - Z_1^2\sec n\theta\tan n\theta_c \tag{3c}$$

$$Z_T \times Z_{oo}(f_2) = -Z_T Z_1\tan n\theta\cot n\theta_c - Z_1^2\sec n\theta\cot n\theta_c \tag{3d}$$

One can validate that $Z_{oe}(f_1)Z_{oo}(f_1) = Z_{oe}(f_2)Z_{oo}(f_2) = Z_1^2$ when $Z_1 = Z_T$. Here, the dispersion of microstrip characteristic impedance is neglected. Once n, θ_c and θ are given, by enforcing $Z_{oe}(f_1) = Z_{oe}(f_2)$ or $Z_{oo}(f_1) = Z_{oo}(f_2)$, the structure parameters of the dual-band element can be solved as follows. Figure 2(a) plots the changes of $Z_{oe}(f_1)$ and $Z_{oe}(f_2)$ with respect to the variation of θ for $\theta_c = 50^o$, 47.5^o and 45^o for $n = 2.12$. This specific n value is used when $f_1 = 2.45$ GHz and $f_2 = 5.2$ GHz. As shown in Fig. 2(a), when θ_c is decreased from 50^o to 45^o, the Z_{oe} solution, i.e. the intersected points, is increased. When $\theta_c = 45°$, the solution reads $Z_{oe} = 130\ \Omega$ and $Z_{oo} = 2Z_o^2/Z_{oe} = 38.45\ \Omega$. Implemented by coupled microstrips, the gap size over substrate thickness ratio S/h will be 0.08 for a substrate with $\varepsilon_r = 10.2$. When the substrate thickness $h = 1$ mm, such gap sizes will be critical for microstrip realization by the standard fabrication process since it is close to being beyond the resolution limit. One may increase θ_c to release the tight gap size as indicated in Fig. 2(a). Figure 2(b) draws the $Z_{oe}(f_1)$ and $Z_{oe}(f_2)$ solutions against the variation of θ for $n = 2.1, 2.2, \ldots, 3$ for $\theta_c = 45°$. When n is increased, the Z_{oe} solution decreases. Note that when $\theta = 0$ and $n = 3$, the solution $Z_{oe} = 70.7\ \Omega$. It validates the fact that when the two-port is used to imitate a λ/4 section at f_1 and 3λ/4 at $f_2 = 3f_1$, the *C*-section becomes a folded section with $Z_{oe} = Z_{oo}$.

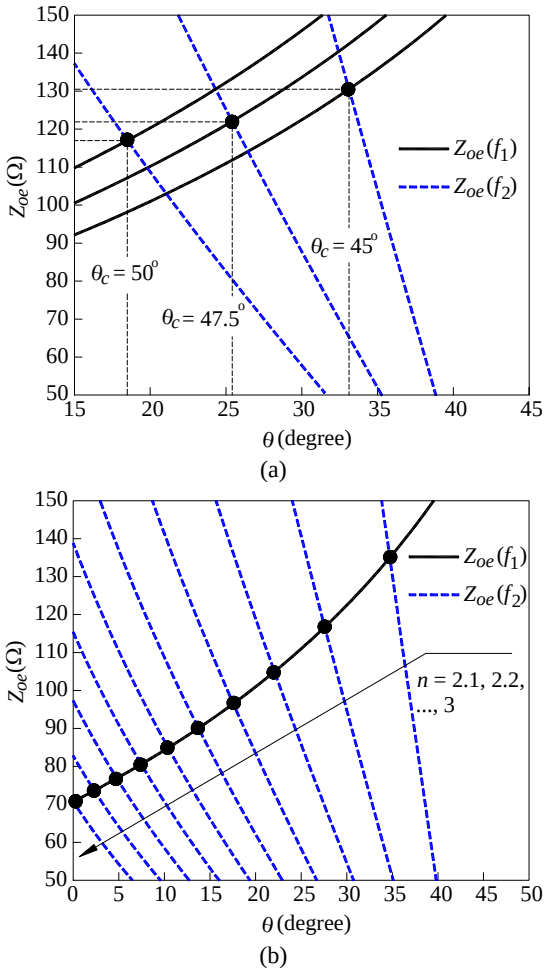

Fig. 2. $Z_{oe}(f_1)$ and $Z_{oe}(f_2)$ against the variation of θ, where $Z_1 = 70.7\ \Omega$. (a) $n = 2.12$. (b) $\theta_c = 45°$.

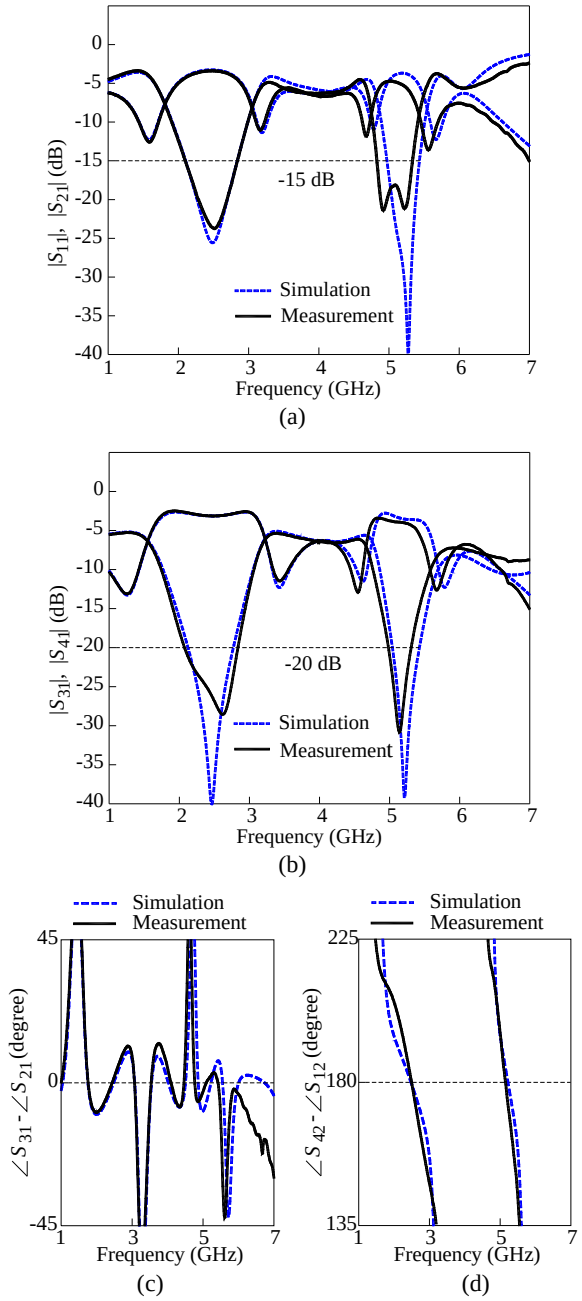

Fig. 3. Simulated and measured responses of the fabricated rat-race coupler at 2.45/5.2 GHz. (a) $|S_{11}|$ and $|S_{21}|$. (b) $|S_{31}|$ and $|S_{41}|$. (c) $\angle S_{31} - \angle S_{21}$. (d) $\angle S_{42} - \angle S_{12}$. n = 2.12, θ_c = 48°, θ = 23.85°, Z_1 = 70.7 Ω, Z_{oe} = 120.65 Ω and Z_{oo} = 41.45 Ω.

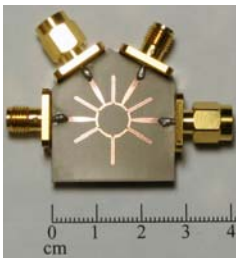

Fig. 4. Photograph of the dual-band rat-race.

III. Simulation and Measurement

Two rat-race couplers designed at 2.45/5.2 GHz and 2.45/5.8 GHz are fabricated and measured for demonstration Figures 3 and 4 show the simulated and measured results. The circuit has a substrate of ε_r = 10.2 and h = 1.27 mm. Simulation data are obtained by the electromagnetic software package IE3D [16]. Figure 3(a) plots $|S_{11}|$ and $|S_{21}|$ responses. It can be observed that all measured $|S_{11}|$ at both the designated frequencies are better than 18 dB. If a 15-dB return loss is referred, measured data indicate that the circuit has bandwidths of 30% and 9% at f_1 and f_2, respectively. Figure 3(b) shows the $|S_{31}|$ and $|S_{41}|$ curves. The measured isolations $|S_{41}|$ at f_1 and f_2 are better than 25 dB. For a 20-dB reference, the measured isolations possess bandwidths of 27% and 8% at f_1 and f_2, respectively. Also, detailed data show that the total power loss of the circuit $P_L = 1 - |S_{11}|^2 - |S_{21}|^2 - |S_{31}|^2 - |S_{41}|^2$ at f_1 and f_2 are 4% and 8.2%, respectively.

Figure 3(c) and 3(d) plots the responses of relative phase $\angle S_{31} - \angle S_{21}$ and $\angle S_{42} - \angle S_{12}$, respectively. One can observe that these responses have relatively smooth variations over the first band as compared with those over the second. It reflects the fact that the circuit has a bandwidth at f_1 larger than that at f_2. Good agreement between the simulation and measured responses for the experiment circuits can be observed. Figure 4 shows the photograph of the experimental circuit.

Figure 5(a) and 5(b) plots the magnitude responses of S_{11}, S_{21}, S_{31} and S_{41} of the second experimental dual-band rat-race. At both f_1 and f_2, the measured $|S_{11}|$ results are better than 20 dB. The measurement indicates that the circuit has bandwidths of 37% and 8% at f_1 and f_2, respectively, for a 15-dB return loss. These bandwidths are closely related to the relative phases $\angle S_{31} - \angle S_{21}$ and $\angle S_{42} - \angle S_{12}$ shown in Fig. 5(c) and 5(d), respectively. The experimental $|S_{41}|$ data show that the isolations are better than 35 dB, and the total power losses P_L are 3.2% and 7.3% at f_1 and f_2, respectively.

Figure 6 shows the photograph of the experimental circuit. In this design, all the *C*-sections can be placed inside the ring circumference. This is because this circuit has a larger n value than the previous one so that the θ_c solution shown in Fig. 2 can be shorter. It occupies only 31% of the area of a conventional rat-race coupler. It is believed that this circuit has the best size reduction comparing with the microstrip dual-band rat-race couplers in open literature.

IV. Conclusion

The function of a microwave *C*-section is exploited for dual-band and circuit miniaturization operation. For design of a dual-band rat-race coupler, the *C*-section together with two short microstrip sections at its ends is used to replace each of the six λ/4 sections of a traditional coupler at the two design frequencies. This approach can save more than 69% of the circuit area. The proposed two-port is viable for development of other dual-band microwave passive devices.

ACKNOWLEDGEMENT

This work was supported in parts by the ATU program of MoE and by the National Science Council, Taiwan, under the Grant NSC 97-2221-E-009-039.

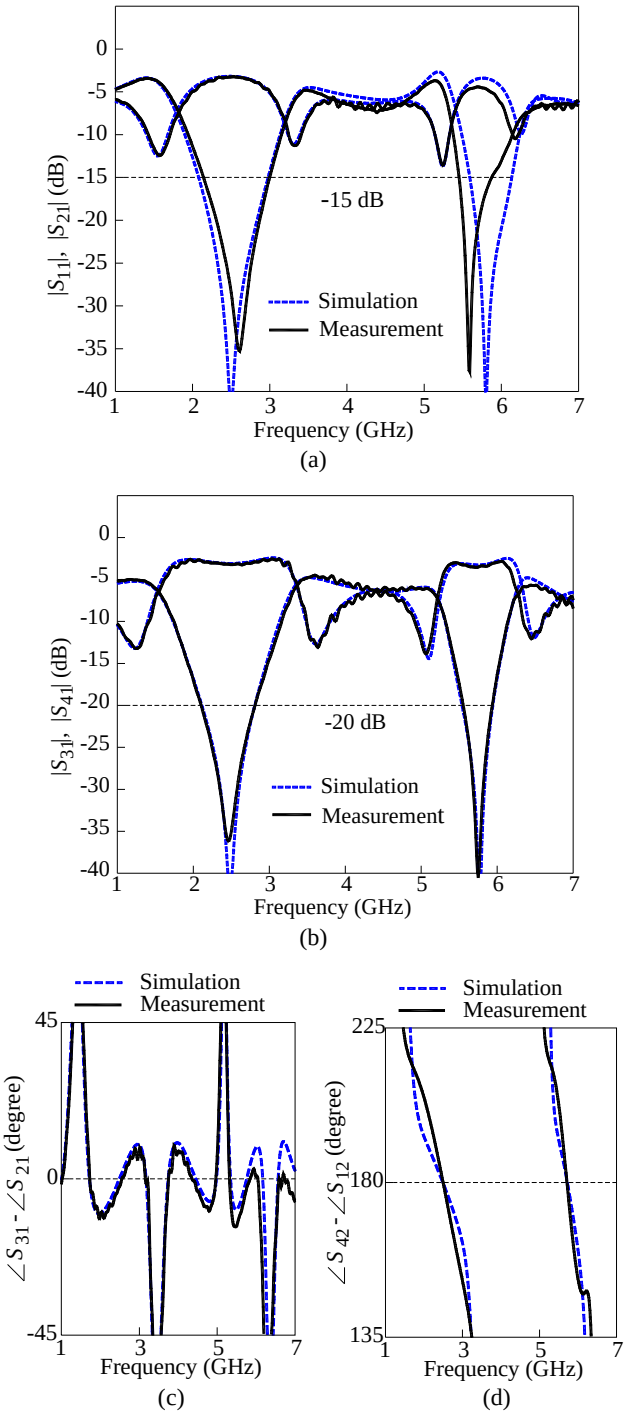

Fig. 5. Simulated and measured responses of the fabricated dual-band rat-race coupler at 2.45/5.8 GHz. (a) $|S_{11}|$ and $|S_{21}|$. (b) $|S_{31}|$ and $|S_{41}|$. (c) $\angle S_{31} - \angle S_{21}$. (d) $\angle S_{42} - \angle S_{12}$. n = 2.37, θ_c = 36.5°, θ = 43.22°, Z_1 = 70.7 Ω, Z_{oe} = 121 Ω and Z_{oo} = 41.33 Ω.

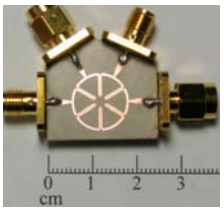

Fig. 6. Photograph of the fabricated 2.45/5.8 GHz rat-race coupler.

REFERENCES

[1] D. M. Pozar, *Microwave Engineering*, 3rd ed. New York: Wiley, 2005.

[2] C. Y. Pon, "Hybrid-ring directional coupler for arbitrary power division," *IEEE Trans. Microw. Theory Tech.*, vol. 19, no. 11, pp. 529-535, Nov. 1961.

[3] R. Levy and L. J. Lind, "Synthesis of symmetric branch line guide directional couplers," *IEEE Trans. Microw. Theory Tech.*, vol. 16, no. 12, pp. 80-89, Dec. 1968.

[4] A. K. Agrawal and G. F. Mikucki, "A printed-circuit hybrid-ring directional coupler for arbitrary power divisions," *IEEE Trans. Microw. Theory Tech.*, vol. 34, no. 12, pp. 1401-1407, Dec. 1986.

[5] Y.-C. Chiou, J.-S. Wu and Jen-Tsai Kuo, "Periodic stepped-impedance rat race coupler with arbitrary power division," *Proc. 2006 Asia-Pacific Microw. Conf.*, pp. 663-666, Dec. 2006.

[6] K.-K. M. Cheng and F.-L. Wong, "A novel approach to the design and implementation of dual-band compact planar 90° branch-line coupler," *IEEE Trans. Microw. Theory Tech.*, vol. 52, no. 11, pp. 2458-2463, Nov. 2004.

[7] K.-K. M. Cheng and F.-L. Wong, "A novel rat race coupler design for dual-band applications," *IEEE Microw. Wireless Compon. Lett.*, vol. 15, no. 8, pp. 521-523, Aug. 2005.

[8] M.-J. Park and B. Lee, "Dual-band cross-coupled branch line coupler," *IEEE Microw. Wireless Compon. Lett.*, vol. 15, no. 10, pp. 655-657, Oct. 2005.

[9] H. Zhang and K. J. Chen, "A stub tapped branch-line coupler for dual-band operations," *IEEE Microw. Wireless Compon. Lett.*, vol. 17, no. 2, pp. 106-108, Feb. 2007.

[10] C.-L. Hsu, C.-W. Chang and J.-T. Kuo, "Design of dual-band microstrip rat race coupler with circuit miniaturization," *IEEE MTT-S Int. Microw. Symp. Dig.*, pp. 177-180, Jun. 2007.

[11] S. Y. Zheng, S. H. Yeung, W. S. Chan, K. F. Man, S. H. Leung and Q. Xue, "Dual-band rectangular patch hybrid coupler," *IEEE Trans. Microw. Theory Tech.*, vol. 56, no. 71, pp. 1721-1728, Jul. 2008.

[12] I.-H. Lin, M. Devincentis, C. Caloz and T. Itoh, "Arbitrary dual-band components using composite right/left-handed transmission lines," *IEEE Trans. Microw. Theory Tech.*, vol. 52, no.4, pp. 1142-1149, Apr. 2004.

[13] X. Q. Lin, R. P. Liu, X. M. Yang, J. X. Chen, X. X. Ying, Q. Cheng and T. J. Cui, "Arbitrary dual-band components using simplified structures of conventional CRLH TLs," *IEEE Trans. Microw. Theory Tech.*, vol. 54, no. 7, pp. 2902-2909, Jul. 2006.

[14] C.-L. Hsu, J.-T. Kuo and C.-W. Chang, "Miniaturized dual-band hybrid couplers with arbitrary power division ratios," to appear in the Jan. 2009 issue of *IEEE Trans. Microw. Theory Tech.*

[15] M. M. Schiffman, "A new class of broad-band microwave 90-degree phase shifter," *IRE Trans. Microw. Theory Tech.*, vol. 6, no. 6, pp. 232-237, Apr. 1958.

[16] *IE3D Simulator*, Zeland Software Inc., Jan. 1997.